



Spike frequency adaptation facilitates the encoding of input gradient in insect olfactory projection neurons

Hayeong Lee^a, Lubomir Kostal^b, Ryohei Kanzaki^c, Ryota Kobayashi^{d,e,f,*}

^a School of Engineering, The University of Tokyo, Tokyo, 113-8656, Japan

^b Institute of Physiology, Czech Academy of Sciences, Prague, 142 20, Czech Republic

^c Research Center for Advanced Science and Technology, The University of Tokyo, Tokyo, 153-8904, Japan

^d Graduate School of Frontier Sciences, The University of Tokyo, Kashiwa, 277-8561, Japan

^e Mathematics and Informatics Center, The University of Tokyo, Tokyo, 113-8656, Japan

^f JST, PRESTO, Saitama, 332-0012, Japan

ARTICLE INFO

Keywords:

Insect olfactory system
Spike frequency adaptation
Input rate-of-change
Sensory coding

ABSTRACT

The olfactory system in insects has evolved to process the dynamic changes in the concentration of food odors or sex pheromones to localize the nutrients or conspecific mating partners. Experimental studies have suggested that projection neurons (PNs) in insects encode not only the stimulus intensity but also its rate-of-change (input gradient). In this study, we aim to develop a simple computational model for a PN to understand the mechanism underlying the coding of the rate-of-change information. We show that the spike frequency adaptation is a potential key mechanism for reproducing the phasic response pattern of the PN in *Drosophila*. We also demonstrate that this adaptation mechanism enables the PN to encode the rate-of-change of the input firing rate. Finally, our model predicts that the PN exhibits the intensity-invariant response for the pulse and ramp odor stimulus. These results suggest that the developed model is useful for investigating the coding principle underlying olfactory information processing in insects.

1. Introduction

The temporal structure of an odor concentration in a natural environment is highly intermittent and dynamic due to atmospheric turbulence (Murlis et al., 1992; Vickers et al., 2001; Celani et al., 2014). The insect olfactory system has evolved to detect the dynamic stimuli in order to process the odorant information for identifying food and mating partners, or for detecting predators (David et al., 1983; Kostal et al., 2008; Semmelhack and Wang, 2009; Álvarez-Salvado et al., 2018; Levakova et al., 2018). In insects, olfactory information is initially encoded by the olfactory receptor neurons (ORNs) (see Wilson, 2013 for a review of early olfactory system). The electric signals generated by ORNs are transmitted to the projection neurons (PNs) in the antennal lobe. These PNs subsequently relay the olfactory information to higher brain centers that process the information and trigger the behavior.

Multiple studies investigated how the olfactory system process the odors (Rosparis et al., 2000, 2003; Hallem and Carlson, 2006; Kanzaki et al., 1989; Sachse and Galizia, 2003; Geffen et al., 2009; Kim et al., 2011, 2015; Fujiwara et al., 2014; Jacob et al., 2017; Levakova et al., 2019). Initially, the researchers analyzed the coding properties of odor concentration in ORNs (Rosparis et al., 2000, 2003; Hallem and Carlson,

2006) and PNs (Kanzaki et al., 1989; Sachse and Galizia, 2003). Subsequently, the advanced recording techniques enabled the researchers to focus on the coding properties of a dynamic odor stimulus (Geffen et al., 2009; Kim et al., 2011, 2015; Fujiwara et al., 2014; Jacob et al., 2017; Levakova et al., 2019). In particular, it was demonstrated that the firing rates of an ORN (Kim et al., 2011) and a PN (Kim et al., 2015; Fujiwara et al., 2014) not only depend on the inputs but also on their rate-of-change (i.e., input gradient: the time derivative of the input).

Neuronal adaptation refers to the change in the responsiveness of the neural system. It also occurs at the cellular level; when a neuron is stimulated by a rectangular current injection, it initially responds with a high firing rate, and then its firing rate decreases. This phenomenon is termed spike frequency adaptation and it is usually mediated by slow K⁺ current, e.g., Ca²⁺-activated K⁺ current I_{KCa} and M-type K⁺ current I_M (Koch, 1999). It has been shown that the multi-timescale adaptive threshold model (MAT model) (Kobayashi et al., 2009) can be derived as a reduced model of the Hodgkin–Huxley model with the slow K⁺ current (Kobayashi and Kitano, 2016). Previous studies reported on the Ca²⁺-activated K⁺ currents I_{KCa} in PNs of honey bees (Grunewald, 2003) and sphinx moths (Mercer and Hildebrand, 2002). Few studies (Farkhooi et al., 2013; Betkiewicz et al., 2020) have incorporated

* Corresponding author at: Graduate School of Frontier Sciences, The University of Tokyo, Kashiwa, 277-8561, Japan.
E-mail address: r-koba@k.u-tokyo.ac.jp (R. Kobayashi).

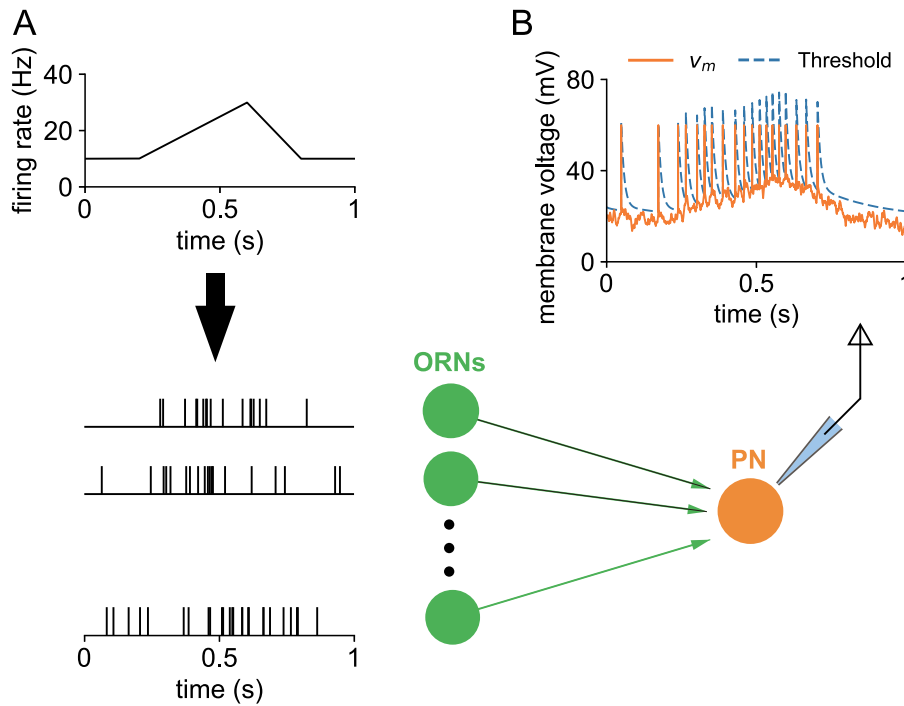


Fig. 1. Model of a projection neuron in *Drosophila*. Our model consists of the olfactory receptor neurons (ORNs) and a projection neuron (PN) as follows:

(A) Input (ORNs): The spiking activity of ORNs (bottom) was generated by an Poisson process with a time-varying firing rate (top).

(B) Projection neuron: A PN is described as an integrate-and-fire model with adaptive spike threshold (MAT model (Kobayashi et al., 2009)). The PN model generates a spike train in response to a stimulus.

the spike frequency adaptation into the computational model of the PNs and simulated the insect olfactory system. These studies suggest that the spike frequency adaptation promotes the reliable and sparse coding. However, there is limited information on its role in encoding a dynamic odor stimulus.

In this paper, we develop a simple computational model for a PN based on the MAT model that is a minimal model incorporating the spike frequency adaptation. We tested whether this model can reproduce a phasic response pattern of the PN recorded from *Drosophila* (Kim et al., 2015). Furthermore, we examine the role of spike frequency adaptation in encoding the rate-of-change information. Finally, we simulate the PN response to the rescaled ORN inputs by using the developed model. The result suggests that dynamic odor encoding in PNs has an intensity-invariant property.

2. Methods

2.1. Model of a projection neuron in *Drosophila*

We simulated a spiking neural network model with two layers, namely the olfactory receptor neurons and the projection neuron (Fig. 1). This model consisted of 300 olfactory receptor neurons (ORNs) and a projection neuron (PN). The connections between the layers were feedforward and excitatory. We modeled the ORNs as independent Poisson spike generators (Betkiewicz et al., 2020), i.e., the spike trains were generated using a Poisson process with time-dependent intensity (firing rate) $r_{\text{ORN}}(t)$.

The PN was modeled either as the standard integrate-and-fire (LIF) neuron (Bugmann et al., 1997; Sacerdote and Giraudo, 2013; Dayan and Abbott, 2005) or as an integrated-and-fire neuron with adaptive spike threshold (MAT model) (Kobayashi et al., 2009; Kobayashi and Kitano, 2016) that accounted for the spike-frequency adaptation. In the following, we describe the MAT neuron model (see Appendix A for

the description of the LIF model). The membrane voltage $v_m(t)$ of the neuron obeys the following equation:

$$\tau_m \frac{dv_m(t)}{dt} = -(v_m(t) - V_L) + RI_{\text{syn}}(t), \quad (2.1)$$

where τ_m is the membrane time constant, V_L is the leak potential, and R is the membrane resistance. The synaptic current $I_{\text{syn}}(t)$ from ORNs is given by (Dayan and Abbott, 2005; Lánská et al., 1994)

$$I_{\text{syn}}(t) = -g_{\text{syn}}(t)(v_m - V_E), \quad (2.2)$$

where V_E is the excitatory reversal potential. The total synaptic conductance $g_{\text{syn}}(t)$ obeys the following equation (Betkiewicz et al., 2020; Dayan and Abbott, 2005):

$$\frac{dg_{\text{syn}}(t)}{dt} = -\frac{g_{\text{syn}}(t)}{\tau_E} + \sum_{j=1}^{N_{\text{ORN}}} \sum_k w_{\text{ORN}} \delta(t - t_{j,k}^{\text{ORN}}), \quad (2.3)$$

where τ_E is the synaptic time constant, $N_{\text{ORN}} = 300$ is the number of ORNs, $w_{\text{ORN}} = 1.4$ nS is the synaptic conductance from an ORN to the PN, and $t_{j,k}^{\text{ORN}}$ represents the k th spike's time of the j th ORN. This value of the synaptic conductance w_{ORN} resulted in excitatory postsynaptic potentials (EPSPs) with amplitudes of 1.0 mV at the resting membrane voltage (Kobayashi and Kitano, 2013).

The MAT neuron generates a spike when the voltage reaches the dynamic spike threshold $\theta(t)$ as follows:

$$\theta(t) = \omega + \sum_{t_k < t} \eta(t - t_k), \quad (2.4)$$

where ω is a constant and the summation is calculated over all PN spike times, t_k , up to time t . The threshold kernel function, $\eta(t)$, is given as the sum of two exponential functions as follows:

$$\eta(t) = \begin{cases} 0 & \text{for } t < 0 \\ \alpha_1 e^{-t/\tau_1} + \alpha_2 e^{-t/\tau_2} & \text{otherwise.} \end{cases} \quad (2.5)$$

The MAT model does not reset the voltage after the spike, unlike the LIF model (Appendix A); however, the spike threshold increases after

Table 1
Hyper-parameters used for fitting the parameters.

Parameter	Initial point	Lower bound	Upper bound
α_1	20 mV	0 mV	100 mV
α_2	2 mV	0 mV	100 mV
ω	20 mV	19 mV	27.5 mV
τ_1	10 ms	1 ms	20 ms
τ_2	200 ms	100 ms	2000 ms

each spike. In the original MAT model (Kobayashi et al., 2009), the threshold-kernel is given by the sum of multiple exponential decaying components. In this study, the number of decaying components was determined based on leave-one-out cross-validation (Appendix B). When the neuron fires, the threshold instantly increases by $\alpha_1 + \alpha_2$ and it subsequently decays according to the time constants (τ_1 and τ_2). In addition, the MAT model includes an absolute refractory period, i.e., the neuron cannot spike during period t_{ref} after previous spike. The threshold parameters $\{\omega; \alpha_1, \alpha_2; \tau_1, \tau_2\}$ were fitted from the experimental data (see Section 2.2 for details), whereas the remaining parameters were fixed. Table 2 summarizes the parameters of the model.

The simulation codes were written in Python. Eqs. (2.1) and (2.3) are integrated by using Euler method with a time step of 0.1 ms. To achieve the steady-state conditions, we simulated the model for 1.0 s before recording the activity. The simulation code shall be made available upon request from the corresponding author.

2.2. Fitting procedure

We fitted the threshold parameters $\mathbf{q} = \{\omega; \alpha_1, \alpha_2; \tau_1, \tau_2\}$ to reproduce the dynamics of the PN firing rate recorded from *Drosophila* (Kim et al., 2015). In this experiment, the authors recorded the response of the PN (DM4) and ORN (Or59b) to an odor stimuli (acetone) with three types of time-varying concentration (a pulse, a ramp, and a parabola waveform) were recorded from the $n = 5$ flies. We extracted the average firing rates of the PNs and ORNs from the paper (Fig. 2 in Kim et al., 2015) using Webplotdigitizer (Rohatgi, 2021).

We determined the optimal values of the threshold parameters by minimizing the sum of the mean squared error over the mentioned three response types (pulse, ramp, parabolic waveform),

$$\hat{\mathbf{q}} = \underset{\mathbf{q}}{\operatorname{argmin}} [E_1 + E_2 + E_3], \quad (2.6)$$

where E_j is the mean squared error and $j = 1, 2, 3$ indexes the response type. Specifically,

$$E_j = \frac{1}{N_{obs}} \sum_t \left\{ r_j^D(t) - r_j^M(t) \right\}^2, \quad (2.7)$$

where $r_j^D(t)$ and $r_j^M(t)$ are the firing rate of the PN calculated from the experimental data and the firing rate of the PN calculated from the model, respectively, and N_{obs} is the number of observation points. We simulated the model for 25 trials with a specified ORN firing rate, and calculated the PN firing rate $r_j^M(t)$ by constructing a peristimulus time histogram (PSTH) using the sliding window method. The window size was 100 ms, and the window was moved with a constant interval of 25 ms (Kim et al., 2015). We used the Nelder–Mead method (Nelder and Mead, 1965) for the minimization. Table 1 summarizes the values of the hyperparameters used for the optimization.

3. Results

3.1. Simple neuron model for a projection neuron in *Drosophila*

We developed a simple model that reproduces the response patterns of a projection neuron (PN) in *Drosophila* (Fig. 1). This model consists of two layers, namely ORNs and a single PN. The input layer consists of 300 ORNs modeled as a Poisson spike generator with the firing

Table 2
Parameters of the projection neuron model.

Neuron parameters			fitted/fixed
Membrane time constant	τ_m	5 ms	fixed (Kobayashi et al., 2009; Nagel et al., 2015)
Membrane resistance	R	50 M Ω	fixed (Kobayashi et al., 2009)
Leak reversal potential	V_L	0 mV	fixed (Kobayashi et al., 2009)
Refractory period	t_{ref}	2 ms	fixed (Kobayashi et al., 2009)
Weight of adaptation	α_1	13.6 mV	fitted
Weight of adaptation	α_2	0.477 mV	fitted
Asymptotic value of threshold	ω	20.4 mV	fitted
Adaptation time constant	τ_1	10.1 ms	fitted
Adaptation time constant	τ_2	805 ms	fitted
Synaptic parameters			
Synaptic weight	w_{ORN}	1.4 nS	fixed (Kobayashi and Kitano, 2013)
Excitatory reversal potential	V_E	65 mV	fixed (Betkiewicz et al., 2020)
Excitatory time constant	τ_E	2 ms	fixed (Betkiewicz et al., 2020)
Number of ORNs	N_{ORN}	300	fixed

Table 3

Fitting error (mean squared error). Bold letters indicate that the error is significantly smaller.

	LIF	MAT
Peaked input: Fig. 2D	449 \pm 3.0	202 \pm 2.5
Rectangular input: Fig. 2E	1814 \pm 4.1	181 \pm 3.8
Ramp input: Fig. 2F	2991 \pm 6.8	493 \pm 5.6

rate $r_{ORN}(t)$. The PN is described either by the standard LIF model, or the LIF model with an adaptive spike threshold (denoted as MAT model) (Kobayashi et al., 2009).

We validated the proposed models by analyzing the experimental data from *Drosophila* (Kim et al., 2015). Fig. 2 depicts the average firing rate $r_{ORN}(t)$ of ORNs (Or59b) (Fig. 2 A, B, and C), and the rate $r_{PN}(t)$ of PNs (DM4) (Fig. 2 D, E, and F) for three types of time-varying stimulus estimated from the experimental data. We examined if the MAT model (see Section 2.1) can reproduce the firing rate of the PN in response to the input firing rate $r_{ORN}(t)$. This model accurately reproduces the time course of the PN responses for each stimulus condition (Fig. 2 D, E, and F, magenta lines).

Table 2 summarizes the model parameters. The majority of parameters were adopted from previous studies (Kobayashi et al., 2009; Betkiewicz et al., 2020; Kobayashi and Kitano, 2013; Nagel et al., 2015), whereas the number of ORNs N_{ORN} was selected to reproduce the spontaneous firing rate of a PN (Kim et al., 2015; Perez-Orive et al., 2002; Krofczik et al., 2009). We determined the parameters of the spike threshold (responsible for the spike frequency adaptation) by minimizing the squared error between the model firing rate and the data (see Section 2.2).

Next, we examine the importance of the spike frequency adaptation for reproducing the response pattern of the PN. The leaky integrate-and-fire (LIF) model that does not incorporate the spike frequency adaptation was fitted to the same data (see Appendix A for the model and fitting procedure). The LIF model cannot reproduce the peak and the response pattern to the rectangular and ramp input (Fig. 2 E and F). Moreover, its response pattern is always similar to that of the input. Furthermore, we compared the fitting error (Eq. (2.7)) to the experimental data between the model with spike frequency adaptation (MAT model) and the LIF model (Table 3). We calculated the mean and standard deviation of the error from 20 trials. Table 3 demonstrates that the MAT model reproduces the experimental data significantly better than the LIF model for all the cases. Therefore, these results imply that the spike frequency adaptation is essential to reproduce the response pattern of a PN in *Drosophila*.

3.2. Potential mechanism of the rate-of-change coding in PNs

The MAT model can reproduce the response patterns of PNs in *Drosophila* (Fig. 2), which implies that the spike frequency adaptation

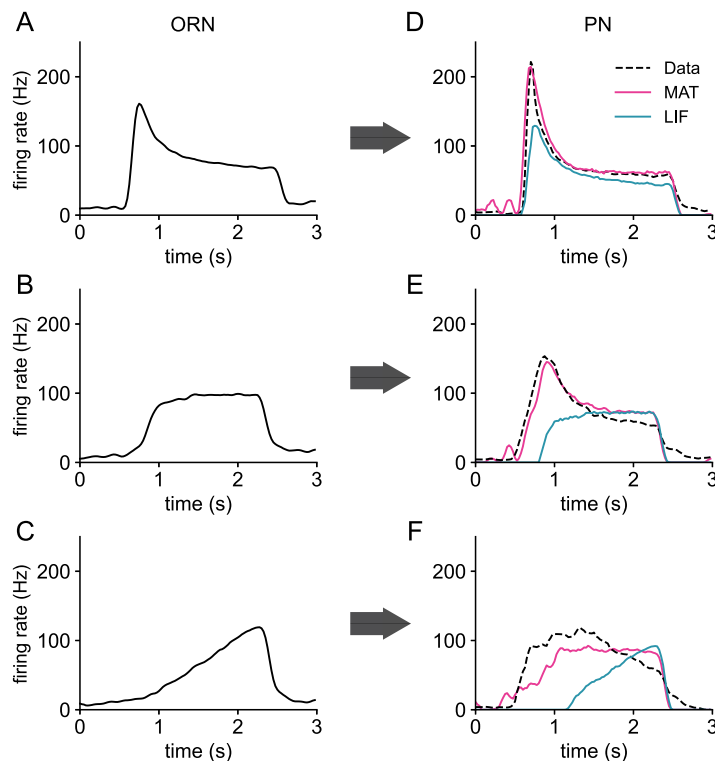


Fig. 2. The model with spike frequency adaption (MAT) can reproduce the response patterns of PNs in *Drosophila*. (A–C) The firing rate of ORNs extracted from the experimental data (Kim et al., 2015). The firing rates are used to generate the spike trains of ORNs. (D–F) The firing rate of a PN. Comparison of average firing patterns of PNs (Kim et al., 2015) (black dashed lines) with the response of the model neurons. Magenta and cyan lines represent the firing rate of the MAT and LIF model, respectively.

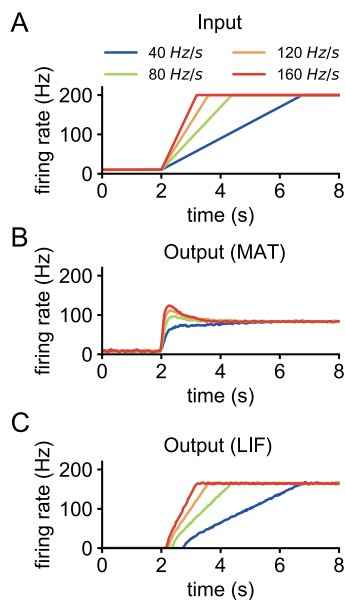


Fig. 3. The MAT model can encode the rate-of-change of the input firing rate. (A) Firing rate of the input neurons. The firing rate linearly increases from the spontaneous firing rate (10 Hz) to the maximum one (200 Hz). (B), (C) Firing rate of the model neurons: (B) MAT and (C) LIF model neuron. Colors of lines represent the levels of the rate-of-change.

is an essential factor to reproduce the experimental data (Table 3). An experimental study suggests that a PN in *Drosophila* encodes not only the firing rate of the ORN (input neuron) but also its rate-of-change (input gradient) (Kim et al., 2015). In this subsection, we examined the

effect of spike frequency adaption on the encoding of the rate-of-change information.

We considered a piece-wise linear input firing rate (Fig. 3A) as follows:

$$r_{in}(t) = \begin{cases} r_{sp} & \text{for } t \leq t_{st} \\ r_{sp} + s(t - t_{st}) & \text{for } t_{st} < t < t_{en} \\ r_{max} & \text{otherwise,} \end{cases} \quad (3.1)$$

where $r_{sp} = 10$ Hz is the spontaneous firing rate, $r_{max} = 200$ Hz is the maximum firing rate, s represents the rate-of-change (slope) of the firing rate, and t_{st} is the start time of a stimulus.

We compared the response of the MAT model neuron with that of the LIF model neuron. First we considered the MAT model that incorporates the spike frequency adaption. The MAT model converges to a constant firing rate in 2 s following the stimulus onset for all the stimuli (Fig. 3B). For the stimulus with a high rate-of-change (≥ 80 Hz/s), the model exhibits a “phasic” response, that is, the firing rate exhibits a peak and subsequently converges to the constant level. For the stimulus with a low rate-of-change (≤ 40 Hz/s), the model does not exhibit an obvious peak. In contrast, the response pattern of the LIF model is similar to that of the input firing rate (Fig. 3C). In addition, we observe that the MAT model responses more rapidly to the stimulus onset than the LIF model. This result implies that the spike frequency adaption enables the neuron to encode the rate-of-change of the input firing rate using a peak (Fig. 3B).

We examined how the MAT model and the LIF model encode the rise of the input firing rate using the piece-wise linear signal (Fig. 3A). Fig. 4 shows how the model neurons transform the input firing rate into the output firing rate. We calculated the output firing rate by constructing the PSTH (Section 2.2). For a low input firing rate (< 20 Hz), the slope between input and output firing rate of the MAT model (Fig. 4A) is steep. However, the output firing rate of LIF model remains zero when

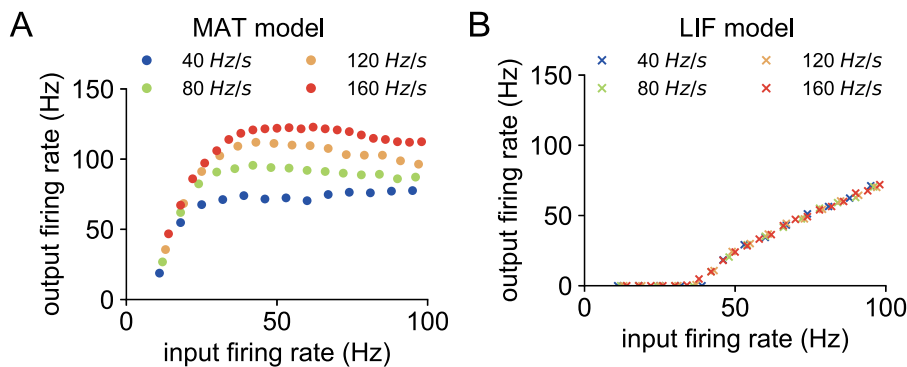


Fig. 4. Coding the stimulus onset in model neurons. Scatter plots in which each point represents the input firing rate and output firing rate of the model neuron at the same time. Two model neurons were examined, namely (A) MAT model and (B) LIF model. Colors of points represent the rate-of-change of the input.

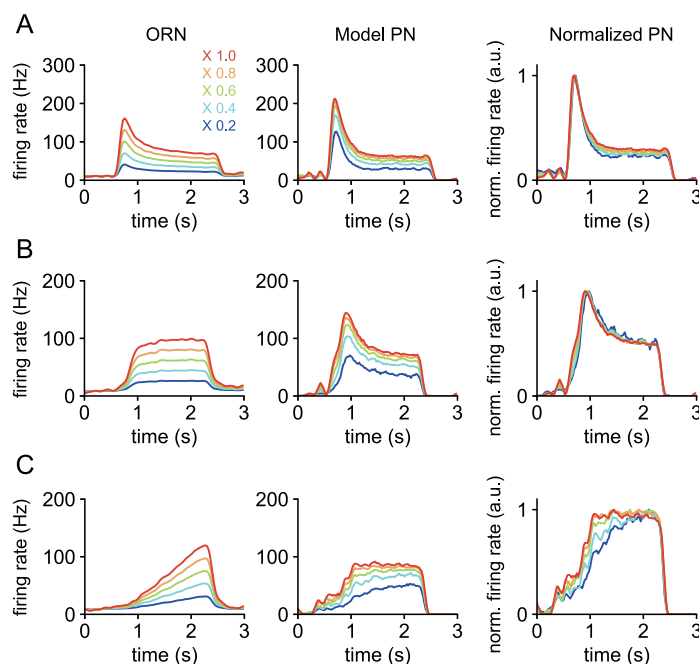


Fig. 5. Intensity-invariant response of the PN model. Responses of the PN model to the rescaled (A) pulse, (B) ramp, and (C) parabolic odor stimulus. The left panels show the scaled ORN activity corresponding to the response to a rescaled odor stimulus. The ORN firing rates are scaled by constant factors (from 0.2 to 1.0 with the step of 0.2) after subtracting the spontaneous activity. The center and right panels show the PN model responses, and their normalization based on the peak values, respectively.

a input firing rate is lower than 40 Hz (Fig. 4B). In other words, the output gain of the MAT model is higher than the LIF model. In addition, the firing rate of the MAT model does not depend on the input firing rate for a high input regime (> 30 Hz), but it depends on the input rate-of-change (Fig. 4A). It means that a similar input firing rate results in a different output firing rate in the MAT model, depending on the rate-of-change of the input. By contrast, a particular input rate gives always the same output rate for the LIF model, which is independent of the input rate-of-change (Fig. 4B). Note that the result in Fig. 4B was obtained by employing the optimal model parameters (see Appendix A for the LIF model). It is possible to make the LIF neuron more sensitive (firing for low input rates), e.g., by decreasing the threshold θ_V , but the qualitative consequences would remain the same, that is, the LIF model cannot encode the rate-of-change input information. Thus, these results suggest that the spike-frequency adaptation enables the neuron to encode the rate-of-change of the input.

It is known that a single neuron exhibits a high-pass filtering property when it encodes the visual stimulus (Victor and Shapley, 1979). Furthermore, it has been shown that the spike frequency adaptation contributes to the high-pass filtering property (Benda and Herz, 2003). Here, we show that the spike frequency adaptation facilitates the

neuron encoding of the input rate-of-change (i.e., the differential of the input). Note that the differentiator is a special case of the high-pass filter, but they are not equivalent. In this study, we have shown that the MAT model with the parameters fitted from PN data achieves the differentiator property in addition to the high-pass filter property.

3.3. PN model exhibits intensity invariant response

A previous study (Martelli et al., 2013) showed that the shape of the ORN response pattern (or response dynamics) is remarkably invariant to the intensity of the odor concentration. Specifically, the ORN responses to the stimuli with equal timescales and dynamics but different intensities were the same when normalized to the peak firing rate (Martelli et al., 2013, Fig. 10b, c). The authors concluded that the response invariance to stimulus intensity is a robust feature of ORNs in *Drosophila*. We investigated a similar question using our PN model (described in Section 2.1), i.e., whether the response invariance to stimulus intensity is also a feature of the PNs. We simulated the ORN response to the odor stimulus with the same dynamics but with a different intensity, and we use this response as the input to the PN model. In particular, we obtained the ORN activity by rescaling the

Table A.1
Hyper-parameters used for fitting the LIF model.

Parameter	Initial value	Lower bound	Upper bound
τ_m	10 ms	0.1 ms	100 ms
θ_V	15 mV	5 mV	100 mV
v_{res}	5 mV	-100 mV	100 mV

ORN firing rate extracted from experimental data (Fig. 2A–C), after the removal of the spontaneous activity.

Fig. 5 shows that the model PN response is intensity-invariant for the (A) pulse and (B) ramp stimulus when the output firing rate is rescaled to its peak rate (as in Martelli et al., 2013). In contrast, the PN response does not exhibit the intensity-invariant property for the (C) parabolic odor stimulus. We observed that the LIF model neuron exhibits the intensity-invariant response property similar to the PN model (Appendix C). The result suggests that the intensity-invariant property highly depends on the temporal pattern of the input rather than the neuronal property. The intensity-invariant property of a neuron can be explained by the linearity of the stimulus–response curve. If the stimulus–response curve is the simple linear function: $r(s) = As$ (s represents the input stimulus), we can expect that the response to a rescaled stimulus cs (c represents the scaling factor) is also rescaled: $r(cs) = cr(s)$. Indeed, the previous studies (Ermentrout, 1998; Kobayashi, 2009) suggest that the stimulus–response curve of the LIF model is asymptotically linear in the strong input regime, and the spike frequency adaptation in the MAT model linearizes its stimulus–response curve in the weak input regime.

In addition, the PN response is approximately invariant *already* on the actual firing rate when the input is relatively high (the scaling factor is larger than 0.6 in Fig. 5). In other words, the PN response exhibits an intensity-invariant feature without normalizing the firing rate, while the ORN response still encodes the overall intensity (Martelli et al., 2013, Fig. 10b, c). Without the normalization, the LIF model neuron does not exhibit the intensity-invariant response (Appendix C). This intensity-invariant property can be explained by the fact that the stimulus–response curve of the MAT model neuron is approximately constant for the strong stimulus (Fig. 4A). Therefore, our model predicts that the PN can exhibit the intensity-invariant response for the pulse and ramp odor stimulus. This result also has an implication for coding properties by the ORNs. A previous study suggested that the ORNs in moth exhibit the spike frequency adaptation (Levakova et al., 2019), which implies that the spike frequency adaptation in ORNs also facilitates the differentiator property and the intensity-invariant response in ORNs.

4. Conclusion

In summary, we have presented a simple model that reproduces the phasic response pattern of a PN in *Drosophila*. The MAT model incorporating the spike frequency adaptation reproduces the response pattern, whereas the LIF model cannot. Therefore, the spike frequency adaptation is a potential mechanism for generating the phasic response. In addition, we demonstrate that the spike frequency adaptation facilitates the neuron to encode dynamic inputs in two ways. First, it improves the ability to signal the small input change. Second, it enables the neuron to encode the input rate-of-change using the peak firing rate. These results suggest that the spike frequency adaptation facilitates the neuron to encode the rate-of-change information. Finally, our model predicts that the PN exhibits the intensity-invariant response for the pulse and ramp odor stimulus. Future studies can focus on testing these predictions and their implications on olfactory information processing in insects.

Table B.1

Cross-validation errors of the MAT model with all the combinations of the time constants. The best result is shown in bold.

	Number of components	Time constant(s)	CV error
1		10 ms	3031 ± 9.0
		100 ms	2652 ± 8.3
		1000 ms	5372 ± 40
2		10, 100 ms	2963 ± 9.0
		10, 1000 ms	1354 ± 9.1
		100, 1000 ms	4640 ± 37
3		10, 100, 1000 ms	1462 ± 10

Declaration of competing interest

The authors declare the following financial interests/personal relationships which may be considered as potential competing interests: Lubomir Kostal is supported by the Czech Science Foundation, and Ryota Kobayashi is supported by JSPS KAKENHI, JST PRESTO, and AMED. These funders had no role in the design of this study, the development of the model, data analysis, data interpretation, and writing the manuscript.

Data availability

Data will be made available on request.

Acknowledgments

We thank Tomoki Kazawa and Stephan Shuichi Haupt for the fruitful discussions. This work was supported by the Czech Science Foundation project 20-10251S, JSPS KAKENHI, Japan (No. 18K11560, 19H01133, 21H03559, 21H04571, and 22H03695), AMED, Japan (No. JP21wm0525004), and JST PRESTO (No. JPMJPR1925).

Appendix A. Leaky integrate-and-fire model

We adopted the leaky integrate-and-fire (LIF) model (Dayan and Abbott, 2005), which is one of the simplest models of a neuron. This model does not incorporate the spike-frequency adaptation mechanism. The membrane voltage v_m of the neuron obeys the same Eq. (2.1) as the proposed model:

$$\tau_m \frac{dv_m}{dt} = -(v_m - V_L) + RI_{syn}(t), \quad (\text{A.1})$$

where τ_m is the membrane time constant, $V_L = 0$ mV is the leak potential, $R = 50$ M Ω is the membrane resistance, and $I_{syn}(t)$ is the synaptic currents from ORNs. The synaptic current obeys the same Eqs. (2.2) and (2.3) as the proposed model and the model parameters are also the same.

The spike generation mechanism of the LIF model is different from the proposed model. The model neuron generates spikes when the voltage reaches the spike threshold, $v_m(t) \geq \theta_V$, where θ_V is the constant threshold parameter. If the model generates a spike, the voltage is reset to v_{res} with an absolute refractory period $t_{ref} = 2$ ms.

We fitted the parameters $\mathbf{q} = \{\tau_m, v_{res}, \theta_V\}$ to reproduce the dynamics of the firing rate of a projection neuron recorded from *Drosophila* (Kim et al., 2015). The parameters were determined by minimizing the sum of the squared error (Eq. (2.6)) as with the case of the proposed model. We again used the Nelder–Mead method (Nelder and Mead, 1965). Table A.1 summarizes the hyper-parameters used in the minimization. The following parameters were fitted from the data: $\tau_m = 35.3$ ms, $v_{res} = -21.7$ mV, and $\theta_V = 42.4$ mV.

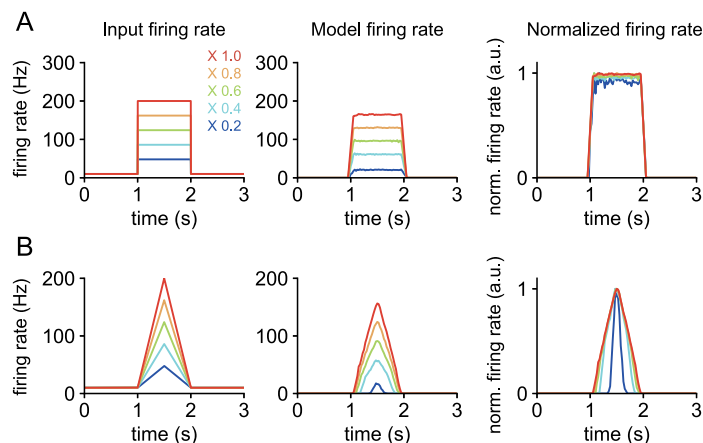


Fig. C.1. Response of the LIF model to the scaled inputs. The LIF model was stimulated with the rescaled (A) step and (B) triangle input firing rate (Left panels). The center and right panels show the model responses (firing rate) and their normalized value based on the peak values, respectively.

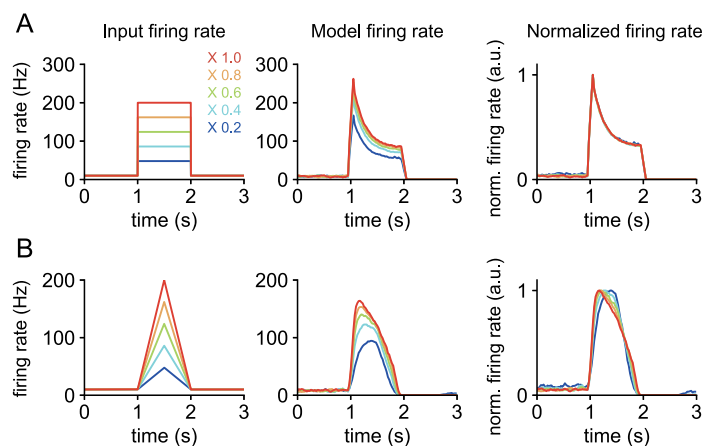


Fig. C.2. Response of the MAT model to the scaled inputs. The MAT model was stimulated with the rescaled (A) step and (B) triangle input firing rate (Left panels). The center and right panels show the model responses (firing rate) and their normalized value based on the peak values, respectively.

Appendix B. Determination of the number of decaying components in the MAT model

In the original MAT model (Kobayashi et al., 2009), the dynamic spike threshold $\theta(t)$ is given by the following equations

$$\theta(t) = \omega + \sum_{k:t_k < t} \eta(t - t_k), \quad (\text{B.1})$$

$$\eta(t) = \begin{cases} 0 & \text{for } t < 0 \\ \sum_{j=1}^L \alpha_j e^{-t/\tau_j} & \text{otherwise,} \end{cases} \quad (\text{B.2})$$

where t_k is the k th spike time, $\eta(t)$ is the threshold-kernel, L is the number of decaying components, and α_j and τ_j ($j = 1, 2, \dots, L$) are the weight and time constant of the j th component, respectively.

Here, we determine the number of components L based on the leave-one-out cross-validation. We calculated the cross-validation error (CV error) with the sum of the error of three types of input waveform (pulse, ramp, and parabola). For each input type, we calculated the mean squared error using the model with the fitted parameters from the remaining two data sets (see Section 2.2 for the fitting procedure).

Table B.1 compares the cross-validation errors of the MAT model with single ($L = 1$), two ($L = 2$), and three ($L = 3$) decaying components. For simplicity, the time constants of the spike threshold were fixed and selected from 10, 100, and 1000 ms. We determined the time constants with the fitting result of the three-component model: $\tau_1 = 10$ ms, $\tau_2 = 93$ ms, and $\tau_3 = 940$ ms. The MAT model with a single

decaying component ($L = 1$) cannot accurately predict the response dynamics of the PNs (Table B.1). The two-component model with $\tau_1 = 10$ ms and $\tau_2 = 1000$ ms achieved minimal error, which suggests the two-component model ($L = 2$) is the best model for predicting the PN response. Thus, we adopted the spike threshold with two decaying components (Eq. (2.5)).

Appendix C. Intensity-invariant response in model neurons

We examine the effect of spike frequency adaptation and the input stimulus on the intensity-invariant response property by simulating two model neurons: the LIF model (Fig. C.1) and MAT model (Fig. C.2). Here, we used the simple input patterns (step and triangle input wave) as the input firing rate to examine essential response properties.

When the output firing rate is normalized, both the LIF and MAT model exhibit the intensity-invariant response for the step input but not for the triangle input (right panels in Figs. C.1 and C.2). This result suggests that the intensity-invariant property in the normalized response is associated with the temporal pattern of the input. For the triangle input, while the LIF model preserves the peak time of the input (Fig. C.1B), the peak time of the MAT model response depends on the input rate-of-change (Fig. C.2B). The high input rate-of-change facilitates the MAT model to respond quickly. Finally, the MAT model neuron approximately achieves the intensity-invariant response without normalization (center panel in Fig. C.2) when the input is relatively high (scale is larger than 0.6 in Fig. 5). The LIF neuron does not exhibit the intensity-invariant response without normalization.

References

- Álvarez-Salvado, E., Licata, A.M., Connor, E.G., McHugh, M.K., King, B.M., Stavropoulos, N., Victor, J.D., Crimaldi, J.P., Nagel, K.I., 2018. Elementary sensory-motor transformations underlying olfactory navigation in walking fruit-flies. *Elife* 7, e37815.
- Benda, J., Herz, A.V., 2003. A universal model for spike-frequency adaptation. *Neural Comput.* 15 (11), 2523–2564.
- Betkiewicz, R., Lindner, B., Nawrot, M.P., 2020. Circuit and cellular mechanisms facilitate the transformation from dense to sparse coding in the insect olfactory system. *Eneuro* 7 (2).
- Bugmann, G., Christodoulou, C., Taylor, J.G., 1997. Role of temporal integration and fluctuation detection in the highly irregular firing of a leaky integrator neuron model with partial reset. *Neural Comput.* 9 (5), 985–1000.
- Celani, A., Villermaux, E., Vergassola, M., 2014. Odor landscapes in turbulent environments. *Phys. Rev. X* 4 (4), 041015.
- David, C., Kennedy, J., Ludlow, A., 1983. Finding of a sex pheromone source by gypsy moths released in the field. *Nature* 303 (5920), 804–806.
- Dayan, P., Abbott, L.F., 2005. *Theoretical Neuroscience: Computational and Mathematical Modeling of Neural Systems*. MIT Press.
- Ermentrout, B., 1998. Linearization of FI curves by adaptation. *Neural Comput.* 10 (7), 1721–1729.
- Farkhooi, F., Froese, A., Muller, E., Menzel, R., Nawrot, M.P., 2013. Cellular adaptation facilitates sparse and reliable coding in sensory pathways. *PLoS Comput. Biol.* 9 (10), e1003251.
- Fujiwara, T., Kazawa, T., Sakurai, T., Fukushima, R., Uchino, K., Yamagata, T., Namiki, S., Haupt, S.S., Kanzaki, R., 2014. Odorant concentration differentiator for intermittent olfactory signals. *J. Neurosci.* 34 (50), 16581–16593.
- Geffen, M.N., Broome, B.M., Laurent, G., Meister, M., 2009. Neural encoding of rapidly fluctuating odors. *Neuron* 61 (4), 570–586.
- Grunewald, B., 2003. Differential expression of voltage-sensitive K⁺ and Ca²⁺ currents in neurons of the honeybee olfactory pathway. *J. Exp. Biol.* 206 (1), 117–129.
- Hallem, E.A., Carlson, J.R., 2006. Coding of odors by a receptor repertoire. *Cell* 125 (1), 143–160.
- Jacob, V., Monsempès, C., Rospars, J.-P., Masson, J.-B., Lucas, P., 2017. Olfactory coding in the turbulent realm. *PLoS Comput. Biol.* 13 (12), e1005870.
- Kanzaki, R., Arbas, E.A., Strausfeld, N.J., Hildebrand, J.G., 1989. Physiology and morphology of projection neurons in the antennal lobe of the male moth *Manduca sexta*. *J. Comp. Physiol. A* 165 (4), 427–453.
- Kim, A.J., Lazar, A.A., Slutskiy, Y.B., 2011. System identification of *Drosophila* olfactory sensory neurons. *J. Comput. Neurosci.* 30 (1), 143–161.
- Kim, A.J., Lazar, A.A., Slutskiy, Y.B., 2015. Projection neurons in *Drosophila* antennal lobes signal the acceleration of odor concentrations. *Elife* 4, e06651.
- Kobayashi, R., 2009. The influence of firing mechanisms on gain modulation. *J. Stat. Mech. Theory Exp.* 2009 (01), P01017.
- Kobayashi, R., Kitano, K., 2013. Impact of network topology on inference of synaptic connectivity from multi-neuronal spike data simulated by a large-scale cortical network model. *J. Comput. Neurosci.* 35 (1), 109–124.
- Kobayashi, R., Kitano, K., 2016. Impact of slow K⁺ currents on spike generation can be described by an adaptive threshold model. *J. Comput. Neurosci.* 40 (3), 347–362.
- Kobayashi, R., Tsubo, Y., Shinomoto, S., 2009. Made-to-order spiking neuron model equipped with a multi-timescale adaptive threshold. *Front. Comput. Neurosci.* 3, 9.
- Koch, C., 1999. *Biophysics of Computation: Information Processing in Single Neurons*. Oxford University Press.
- Kostal, L., Lansky, P., Rospars, J.-P., 2008. Efficient olfactory coding in the pheromone receptor neuron of a moth. *PLoS Comput. Biol.* 4 (4), e1000053.
- Krofczik, S., Menzel, R., Nawrot, M.P., 2009. Rapid odor processing in the honeybee antennal lobe network. *Front. Comput. Neurosci.* 2, 9.
- Lánská, V., Lánský, P., Smith, C.E., 1994. Synaptic transmission in a diffusion model for neural activity. *J. Theoret. Biol.* 166 (4), 393–406.
- Levakova, M., Kostal, L., Monsempès, C., Jacob, V., Lucas, P., 2018. Moth olfactory receptor neurons adjust their encoding efficiency to temporal statistics of pheromone fluctuations. *PLoS Comput. Biol.* 14 (11), e1006586.
- Levakova, M., Kostal, L., Monsempès, C., Lucas, P., Kobayashi, R., 2019. Adaptive integrate-and-fire model reproduces the dynamics of olfactory receptor neuron responses in a moth. *J. R. Soc. Interface* 16 (157), 20190246.
- Martelli, C., Carlson, J.R., Emonet, T., 2013. Intensity invariant dynamics and odor-specific latencies in olfactory receptor neuron response. *J. Neurosci.* 33 (15), 6285–6297.
- Mercer, A.R., Hildebrand, J.G., 2002. Developmental changes in the density of ionic currents in antennal-lobe neurons of the sphinx moth, *Manduca sexta*. *J. Neurophysiol.* 87 (6), 2664–2675.
- Murlis, J., Elkinton, J.S., Carde, R.T., 1992. Odor plumes and how insects use them. *Annu. Rev. Entomol.* 37 (1), 505–532.
- Nagel, K.I., Hong, E.J., Wilson, R.I., 2015. Synaptic and circuit mechanisms promoting broadband transmission of olfactory stimulus dynamics. *Nature Neurosci.* 18 (1), 56–65.
- Nelder, J.A., Mead, R., 1965. A simplex method for function minimization. *Comput. J.* 7 (4), 308–313.
- Perez-Orive, J., Mazor, O., Turner, G.C., Cassenaer, S., Wilson, R.I., Laurent, G., 2002. Oscillations and sparsening of odor representations in the mushroom body. *Science* 297 (5580), 359–365.
- Rohatgi, A., 2021. *Webplotdigitizer: Version 4.5*. URL <https://automeris.io/WebPlotDigitizer>.
- Rospars, J.-P., Lánský, P., Duchamp, A., Duchamp-Viret, P., 2003. Relation between stimulus and response in frog olfactory receptor neurons in vivo. *Eur. J. Neurosci.* 18 (5), 1135–1154.
- Rospars, J.-P., Lánský, P., Duchamp-Viret, P., Duchamp, A., 2000. Spiking frequency versus odorant concentration in olfactory receptor neurons. *Biosystems* 58 (1–3), 133–141.
- Sacerdote, L., Giraud, M.T., 2013. Stochastic integrate and fire models: A review on mathematical methods and their applications. *Stoch. Biomath. Model.* 99–148.
- Sachse, S., Galizia, C.G., 2003. The coding of odour-intensity in the honeybee antennal lobe: Local computation optimizes odour representation. *Eur. J. Neurosci.* 18 (8), 2119–2132.
- Semmelhack, J.L., Wang, J.W., 2009. Select *Drosophila* glomeruli mediate innate olfactory attraction and aversion. *Nature* 459 (7244), 218–223.
- Vickers, N.J., Christensen, T.A., Baker, T.C., Hildebrand, J.G., 2001. Odour-plume dynamics influence the brain's olfactory code. *Nature* 410 (6827), 466–470.
- Victor, J.D., Shapley, R.M., 1979. The nonlinear pathway of Y ganglion cells in the cat retina. *J. Gen. Physiol.* 74 (6), 671–689.
- Wilson, R.I., 2013. Early olfactory processing in *Drosophila*: Mechanisms and principles. *Annu. Rev. Neurosci.* 36, 217–241.